ENVIRONMENTAL ENGINEERING SCIENCE
Volume 38, Number 3, 2021

DOI: 10.1089/ees.2020.0093

Saline Brine Reaction with Fractured Wellbore Cement and Changes in Hardness and Hydraulic Properties

Jorge Gonzalez-Estrella,[1,†] Joshua Ellison,[2] John C. Stormont,[2] Nabil Shaikh,[2] Eric J. Peterson,[3] Peter Lichtner,[2] and José M. Cerrato[2,*,†]

[1]*School of Civil and Environmental Engineering, College of Engineering, Architecture, and Technology, Oklahoma State University, Stillwater, Oklahoma, USA.*
Departments of [2]Civil, Construction and Environmental Engineering and [3]Chemical and Biological Engineering, University of New Mexico, Albuquerque, New Mexico, USA.

Received: March 18, 2020 *Accepted in revised form: September 24, 2020*

Abstract

The integrity of cemented wellbores is fundamental to the containment of subsurface greenhouse gases and hydrocarbons, while minimizing migration of deep subsurface brines. These brines contain salts and hazardous chemicals that could contaminate potable water resources. This study integrated flow measurements, X-ray diffraction, microscopy, and solution chemistry to investigate the physicochemical effects of reacting saline brine waters at circumneutral pH with fractured wellbore cement under varying stress conditions. Chemical reactions of saline brines with cement fracture surfaces can alter the permeability and porosity of the fracture and consequently impact the potential for leakage through the wellbore. Flow measurements on fractured wellbore cement specimens were made with nitrogen, de-ionized water, and finally brine for a range of hydrostatic confining stresses under controlled laboratory conditions. Hydraulic apertures obtained from nitrogen flow measurements decreased in response to the initial increase in confining stress applied to the fracture owing to crushing of asperities. During flow of saline brine, the hydraulic aperture progressively decreased fourfold compared with its unreacted condition. Precipitation of calcite along the flow path likely decreased the hydraulic aperture, limiting the fluid transport through the damaged wellbore system. Our results indicate that saline brine supersaturated with respect to $CaCO_{3(s)}$ promotes precipitation at the wellbore surface showing an initial rapid drop in the fracture aperture followed by a more gradual reduction in the aperture with increasing pore volume. This result suggests injection of brine may reduce leakages of hydrocarbon fluids into the environment.

Keywords: brine; cement; flow; fractured wellbore

Introduction

Cement fractures of wellbores used for oil and gas industry operations pose a risk to the environment and health because of their potential to leak hydrocarbons or brines into freshwater aquifers (Zhang and Bachu, 2011; Phillips *et al.*, 2016) and the atmosphere (Phillips *et al.*, 2016; Garcia-Rios and Gouze, 2018). Leakage also provides a pathway to release greenhouse gases into the environment including carbon dioxide (CO_2) and methane (Kang *et al.*, 2014; Townsend-Small *et al.*, 2016; Schout *et al.*, 2019).

Fractures can be difficult and expensive to repair and affect the functionality of the wellbore (Heathman and East Jr, 1992; Carey *et al.*, 2010). Information is still limited regarding the environmental conditions that affect wellbore cement fractures (i.e., stress, fluid flow, and chemical constituents in both solid and fluids). A better understanding of physicochemical changes in fractured wellbore cement will provide useful information to predict the impact of these fractures.

Fractures in wellbore cements are typically mechanically induced and caused by poor cementing, shrinkage, expansion/contraction, and thermal gradients. Pressure and temperature of fluid inside casing imposing stresses (Wiprut and Zoback, 2000), deformation of adjacent formations (Wiprut and Zoback, 2000; Sobolik and Ehgartner, 2006), or expansion/compaction of underlying reservoirs can change the stress conditions on wellbore cements. Injection of CO_2 following a cyclic pattern can also enlarge the aperture of the fracture (De Andrade *et al.*, 2014).

Interfacial chemical reactions between water and cement can affect the permeability, tortuosity, and porosity of cement. The dissolution/precipitation of portlandite, swelling

**Corresponding author:* Department of Civil, Construction and Environmental Engineering, MSC01 1070, University of New Mexico, Albuquerque, New Mexico 87131, USA. *Phone:* 001-505-277-0870; *Fax:* 001-505-277-1918; *E-mail:* jcerrato@unm.edu
[†]Member of AEESP.

of calcium silica hydrate solids (C–S–H), hydration of nonreacted cement, and adsorption of water (Loosveldt *et al.*, 2002) can decrease cement permeability. Dissolution/precipitation can clog pores and decrease porosity limiting the penetration of fluid through the pores (Brunet *et al.*, 2013). Leaching of calcium from portlandite can increase hydraulic diffusivity (Marchand *et al.*, 2001). Duguid and Scherer (2010) found that calcium-saturated brine did not degrade nor decrease the mechanical properties of cement suggesting that water saturated with calcium prevents the dissolution of portlandite and decalcification of calcium silica hydrate solids (C–S–H). Studies evaluating ammonium nitrate as a surrogate for de-ionized water found that nitrate accelerated the leaching of Ca, increased cement porosity, and decreased its compressive strength (Carde and Francois, 1999; Agostini *et al.*, 2007; Yurtdas *et al.*, 2011a).

A better understanding of coupled physicochemical mechanisms related to the alteration of flow-through cement fractures is necessary to quantify risks associated with wellbores (Carroll *et al.*, 2016). Most studies have focused on the physicochemical effects of acidic brines on fractured cement. Acidic brines, such as those associated with CO_2 sequestration applications, induce reaction zones in cement that alter its mechanical properties (Kutchko *et al.*, 2007; Huerta *et al.*, 2012; Walsh *et al.*, 2014). Acidic brines can cause plastic deformation of asperities, deterioration of mechanical properties of cement (e.g., elastic moduli and hardness) (Huerta *et al.*, 2011; Spokas *et al.*, 2018), and increase the dissolution rates of portlandite (Baur *et al.*, 2004; Marty *et al.*, 2009), which increase the porosity of cement (Kutchko *et al.*, 2007; Huerta *et al.*, 2011; Mason *et al.*, 2013).

Acidity erodes carbonate fracture surfaces and the effect of the acid on the surface depends on the reaction kinetics and flow (Deng and Peters, 2019). Dissolution of the calcium- and carbonate-bearing solids can produce an amorphous-silicate region adjacent to the brine that might increase or decrease fracture permeability (Carey and Lichtner, 2009; Walsh *et al.*, 2014). For instance, mineral precipitation along the fracture at high pH or acidic brine can induce self-sealing (Huerta *et al.*, 2011, 2012; Plattenberger *et al.*, 2020). The amount of precipitation can increase depending on the speed of the flow that goes through the fracture (Nguyen *et al.*, 2020). Research has shown that precipitation by carbonation of calcium and magnesium silicates can seal fractures (Tao *et al.*, 2016; Plattenberger *et al.*, 2020).

Although the body of work concerning reactions at acidic pH constitutes an important foundation, the expected reactions are different for systems involving saline brines at circumneutral pH. The physicochemical alterations potentially occurring in cement fractures from saline brines, such as those that may be associated with hydrofracture flowback waters remain poorly understood (Haluszczak *et al.*, 2013; Vengosh *et al.*, 2014; Ju *et al.*, 2018). This study aims to investigate the physical changes and chemical reactivity that fractured wellbore cement undergoes under confining stress and when reacted with de-ionized water or brine. We used flow measurements, X-ray diffraction, microscopy, and solution chemistry to investigate the physicochemical effects of fractured wellbore cement reacted with nitrogen gas and saline brine waters at circumneutral pH under varying stress conditions. The novel aspect of the experimental approach is that it enables the integrated identification of changes in stress and hydraulic properties caused by mineral dissolution and precipitation in fractured cement. We hypothesize that the reaction of cement with brine will result in dissolution of portlandite and concurrent calcite precipitation causing a decrease in the fracture aperture. The results from this study are relevant to resource extraction applications in which gas and brine fluids interact with cement and can influence wellbore integrity.

Experimental Methods

Sample preparation

A cylindrical wellbore cement sample with a throughgoing fracture along its axis was prepared for this study. This sample was subjected to a sequence of flow tests using nitrogen gas, de-ionized water, and brine; this sample will be referred to as the flow test sample. The nitrogen test was considered a nonreactive fluid, and thus served to establish a baseline for flow measurements for the other fluids. The experiments with de-ionized water were conducted as a chemical control to evaluate the baseline concentration of readily releasable calcium from cement into solution. A fracture creating two halves that were nearly equal in size was developed through tensile-splitting in a Brazilian test configuration. A 0.6 mm thick perforated carbon steel sheet was placed on opposing and opposite ends of the cement core halves to offset the fracture surface, so that the fracture did not perfectly mate when subjected to confinement (Fig. 1).

The carbon steel sheet allowed for reaction with fluid that was injected through the fracture. This sequential flow test was conducted under a range of confining pressures and the effluent was collected for subsequent chemical composition analysis. After the flow test, the hardness and chemical composition of the fracture surface were measured on this cement sample. Another cement sample was prepared in a similar manner for a long-term flow test only with de-ionized water under the same conditions used for the flow test sample.

All cylindrical samples were cast using a ratio of 1,000 g Type I cement, 330 g water, 100 g silica fume, and a 7 g

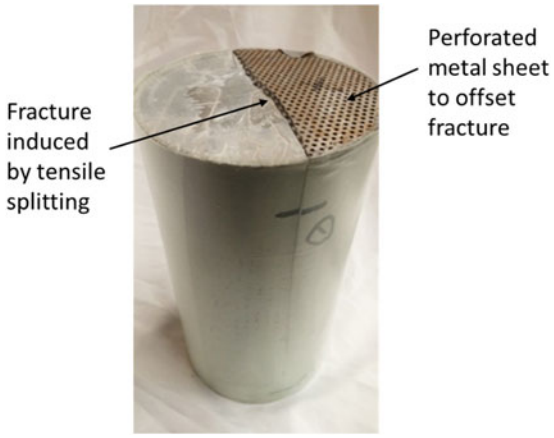

FIG. 1. Fractured cement core (102 mm diameter, 180 mm length) with perforated steel sheet attached to offset the fracture. A similar steel sheet is placed on the *bottom* of the sample on the opposing side of the fracture.

plasticizer, and were cured in a humid environment at 50°C for a minimum of 21 days in accordance with ASTM-International (2014). The cured cylindrical samples had a diameter of 102 mm and a length of 180 mm.

Flow measurements

The flow tests were conducted in a pressure vessel that permitted a hydrostatic confining pressure to be applied to the samples (Fig. 2). Gas flow tests used ultrapure N_2. The upstream gas pressure was controlled with a regulator and measured with a digital pressure gauge. The downstream outlet pressure was atmospheric. Volumetric gas flow was measured using rotameters of different ranges (with ±2% accuracy of total flow range) connected to the downstream side of the specimen.

Liquid flow tests were conducted using a piston pump that supplied water and brine to the upstream side of the sample at flow rates ranging from 0.01 to 10 mL/min. The upstream pressure was measured with a digital pressure gauge. The downstream side was directed to a collection reservoir at atmospheric pressure. The de-ionized water (18 MΩ) used in flow tests was obtained from an ultrapure water dispenser with an initial pH of 5.6. The brine used in flow tests contained (per 1 L of water): 36.75 g of calcium chloride ($CaCl_2$), 117.29 g of sodium chloride (NaCl), and 0.09 g of sodium bicarbonate ($NaHCO_3$) with an initial pH of 8.3. Our brine was prepared based on the concentration range for Ca, Na, Cl, and HCO_3^- in saline flowback samples reported in another study (Haluszczak *et al.*, 2013).

The flow rate through the sample was always more than an order of magnitude greater than that attributable to unreacted cement; consequently, all the flow was assumed to occur through the fracture. The flow data were interpreted as hydraulic aperture (b) of the cement fracture (Witherspoon *et al.*, 1980):

$$b = \left[\frac{12\mu Q}{w\nabla P}\right]^{1/3}, \quad (1)$$

where μ is fluid viscosity, Q is the volumetric flow rate through the fracture, w is the width of fracture, and ∇P is the gradient across the sample. Hydraulic aperture is commonly used to describe fractures in rock and cement (Huerta *et al.*, 2011; Stormont *et al.*, 2018). The fracture permeability, k_f, can be directly derived from the hydraulic aperture ($k_f = b^2/12$). Reynold's numbers were calculated for all flow tests and were found to be well below the critical value where the flow transitions to include a significant inertial flow component (Huitt, 1956; Hassanizadeh and Gray, 1987). Gas slippage (Klinkenberg effect) was not observed in the gas flow measurements because of the relatively large size of the fracture aperture compared with the mean free path of the gas molecules.

Test conditions

The sequence of flow tests including the test fluids and confining stress conditions are given in Table 1. The confining stress was removed and re-applied between flow tests with different fluids. During the flow tests under constant confining stress with de-ionized water and brine (test sequences 3 and 5, respectively), effluent was collected for subsequent chemical analyses. These tests were run for more than 10,000 pore volumes, where a pore volume was taken as the volume of the fracture calculated from the average hydraulic aperture and the sample dimensions.

A second cement sample was only subjected to a long-term flow test with de-ionized water under the same conditions used for the flow test sample described above. This sample was independently analyzed to evaluate the effect of de-ionized water only on the physicochemical response of cement.

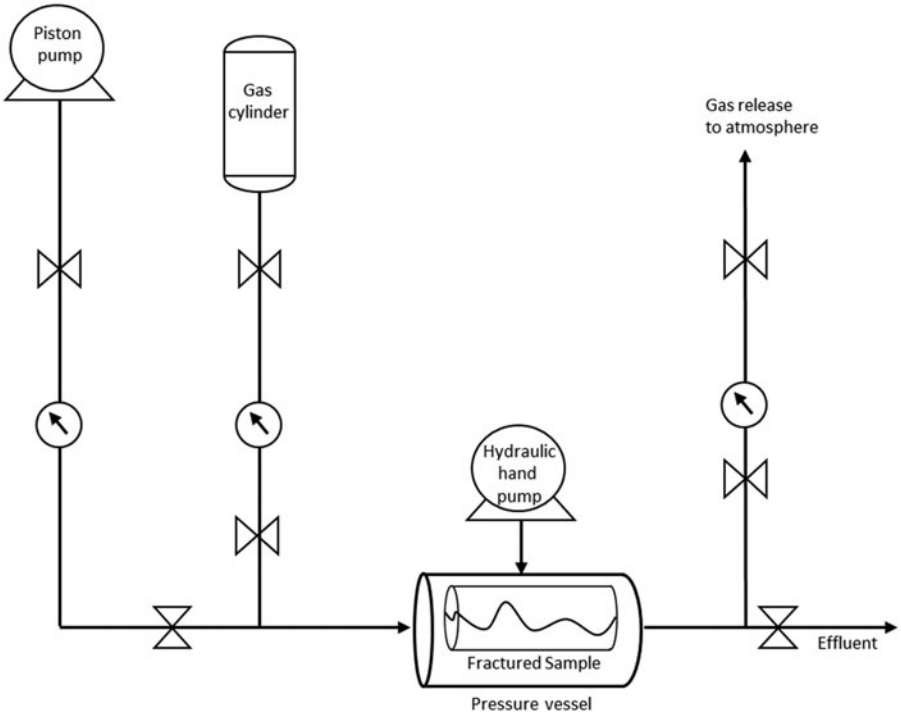

FIG. 2. Experimental set-up for flow test.

Table 1. Flow Test Sequence and Conditions

Flow test sequence	*Flow test fluid*	*Confining stress conditions (MPa)*
1	Nitrogen	Variable between 4.1 and 16.5
2	De-ionized water	Variable between 4.1 and 16.5
3	De-ionized water	Constant at 11
4	Nitrogen	Variable between 4.1 and 16.5
5	Brine	Constant at 11
6	Nitrogen	Variable between 4.1 and 16.5

Hardness measurements of reacted and unreacted fracture surfaces

The hardness values of cement along fracture surfaces were evaluated using micro-hardness values with a Vickers 402 MVD imposing a 300 g force. Fractured surfaces from three different cement cores were evaluated: the flow test sample after conclusion of the flow test sequence given in Table 1, a sample that was only exposed to de-ionized water and the control (unreacted) sample. The measured hardness values of these three samples allows the evaluation of mechanical property alterations after fractures were exposed to brine (the flow sample) and de-ionized water compared with unreacted cement.

Chemical analyses of aqueous and solid samples

Aqueous samples were analyzed using a Perkin-Elmer Optima 5300 DV Inductively Coupled Plasma-Optical Emission Spectrometer (ICP-OES) and a Perkin-Elmer Nexion 300D inductively coupled plasma–mass spectrometer (ICP-MS) system were used to analyze calcium concentrations in aqueous samples. Samples of unreacted and reacted cement with de-ionized water and brine were collected to identify morphology, elemental composition, and mineralogy. Fragments of unreacted and reacted cement samples were prepared for solid analyses by chipping the samples from the fracture faces, making sure that the surface in contact with de-ionized water and brine was preserved as carefully as possible.

Analyses with scanning electron microscopy (SEM; FEI Quanta 3d FEG) integrated with energy dispersive X-ray spectroscopy (EDX; Oxford Instruments INCA) were conducted to identify morphology and chemical composition of areas on the surface (top 1 μm) of the analyzed solids. Diffraction analyses were conducted using a Rigaku Smart Lab X-ray diffractometer (XRD) to identify the crystallinity, mineral structure, and normalized approximate percentage of mineral phases present in bulk solid samples, using Cu K-alpha radiation. The XRD data were analyzed using the Jade® software. The estimated standard deviations (esd) indicating the precision for the quantitative analyses to estimate the weight % of the mineral content, as determined by the Jade software, are given in parentheses in Table 2.

Chemical speciation modeling was performed using MINEQL +4.6 with ionic strength correction based on specific interaction theory (Schecher and McAvoy, 2007; VanBriesen *et al.*, 2010) and FLOTRAN with ionic strength correction using the Pitzer model (Lichtner and Felmy, 2003). These simulations were useful to determine chemical speciation and saturation indices (SIs) for solids that could precipitate under the experimental conditions investigated.

Results and Discussion

Hydraulic response

Hydraulic apertures changed as a function of the fluid (gas or liquid) contacting the wellbore and the confining stress. The hydraulic aperture decreased from 59 to 38.8 μm with confining stress ranging from 5.5 to 16.5 MPa during the first N_2 gas cycle and returned to 39 μm when the confining stress was unloaded to 5.5 MPa (Fig. 3a). During the second cycle of gas flow measurements, the hydraulic aperture varied from 40 to 31 μm with confining stress ranging from 4.1 to 16.5 MPa. The hydraulic aperture returned almost to its initial size (38.5 μm) when the pressure was unloaded. The results of the second cycle showed, therefore, a smaller change in aperture from increase in stress compared with the initial loading and a more elastic response during unloading. The nonrecoverable change in the hydraulic aperture after the initial loading cycle has been widely observed in rock fractures (Bandis *et al.*, 1983; Zhang and Nemcik, 2013; Chen *et al.*, 2015; Zhou *et al.*, 2015) and can be attributed to plastic deformation of asperities of the fracture. Other factors can influence the hydraulic aperture response including flow rate (Elkhoury *et al.*, 2013; Garcia-Rios *et al.*, 2015) or fracture geometry (Deng *et al.*, 2018). For instance, increasing the flow rate may shift the effect on the fracture from compact dissolution to fracture channelization to uniform dissolution (Deng *et al.*, 2018).

A set of flow tests were then made with de-ionized water to compare with the nitrogen gas flow results (Fig. 3b). Measurements of the hydraulic aperture were made with loading path ranging from 5.5 to 16.5 MPa and unloading path returning to 5.5 MPa. The hydraulic aperture decreased from 30 to 22 μm during loading and returned to 30 μm upon unloading. Next, a flow test with de-ionized water was conducted at a constant confining stress of 11 MPa (Fig. 3c). The hydraulic aperture decreased from 29 to 23 μm after 13,000 pore volumes.

Flow tests with nitrogen gas were conducted under the same loading–unloading sequence (5.5 to 16.5 to 5.5 MPa) (Fig. 3d). The hydraulic apertures changed from 29 to 24 μm during loading and returned to 28 μm after unloading. These hydraulic aperture values are similar to those determined from the flow test only with de-ionized water and confirmed that the reduction in hydraulic aperture observed using de-ionized water was permanent and not an artifact of the test fluid.

The subsequent flow measurements were conducted using brine as the test fluid. The confining stress was constant at 11 MPa. The effect of saline brine on the hydraulic aperture was more evident compared with the de-ionized water flow test. The hydraulic aperture changed from 27.5 to 6 μm after 14,500 pore volumes of brine were injected (Fig. 3e). Huerta *et al.* (2011) found similar results in hydraulic apertures in response to brine flow. The postbrine nitrogen gas test confirmed the hydraulic aperture decreased owing to reactivity with brine (Fig. 3f).

Surface hardness comparison for unreacted, de-ionized-reacted, and brine-reacted fractured cement

Hardness was measured on the flow test sample exposed sequentially to nitrogen, de-ionized water, and brine. In addition, hardness measurements were made on the sample that

TABLE 2. X-RAY DIFFRACTOMETER ANALYSIS DATA FOR UNREACTED CEMENT, DE-IONIZED REACTED CEMENT, AND BRINE REACTED CEMENTS

	Unreacted		*De-ionized hard*		*De-ionized soft*		*Brine reacted hard*		*Brine reacted soft*	
Phase Id	*Wt.% (esd)*	*Volume % (esd)*	*Wt.% (esd)*	*Volume % (esd)*	*Wt.% (esd)*	*Volume % (esd)*	*Wt.% (esd)*	*Volume % (esd)*	*Wt.% (esd)*	*Volume % (esd)*
Portlandite $Ca(OH)_2$	9.7 (0.3)	11.4 (0.3)	10.4 (0.3)	12.4 (0.4)	4.6 (0.2)	5.5 (0.3)	4.1 (0.2)	4.9 (0.2)	0.5 (0.0)	0.6 (0.0)
Hatrurite Ca_3SiO_6	14.9 (0.6)	12.3 (0.5)	13.8 (0.6)	11.5 (0.5)	14.1 (0.6)	11.9 (0.5)	10.1 (0.6)	8.5 (0.5)	7.9 (0.6)	6.6 (0.5)
Calcite $CaCO_3$	10.9 (0.4)	10.6 (0.4)	10.7 (0.4)	10.5 (0.4)	14.3 (0.4)	14.2 (0.4)	27.8 (0.5)	27.4 (0.6)	24.8 (0.7)	24.3 (0.7)
Monticellite $CaMgSiO_4$	2.7 (0.4)	2.3 (0.3)	3.6 (0.5)	3.1 (0.4)	3.2 (0.4)	2.7 (0.4)	5.5 (0.5)	4.7 (0.4)	4.4 (0.5)	3.7 (0.4)
$CaAl_4Si_2O_{11}$	0.8 (0.1)	0.6 (0.1)	0.9 (0.1)	0.6 (0.1)	0.7 (0.1)	0.5 (0.1)	0.7 (0.1)	0.5 (0.1)	0.6 (0.1)	0.4 (0.1)
Periclase, syn MgO	1.0 (0.2)	0.7 (0.1)	1.4 (0.2)	1.1 (0.1)	1.7 (0.2)	1.3 (0.1)	0.4 (0.1)	0.3 (0.0)	0.8 (0.2)	0.6 (0.1)
Brownmillerite Ca_2FeAlO_5	4.0 (0.1)	2.8 (0.1)	6.7 (0.4)	4.8 (0.3)	7.5 (0.4)	5.4 (0.3)	3.9 (0.4)	2.8 (0.3)	3.9 (0.4)	2.8 (0.3)
Amorphous + others	56.0 (0.6)	60	52.4 (0.6)	59.5	54.0 (0.6)	58.5	47.5 (0.6)	50.9	57.1 (0.7)	61

Quantity in parenthesis is esd.
esd, estimated standard deviation.

was only exposed to de-ionized water and on the unreacted sample (control). Overall, the reacted samples showed lower Vickers hardness values compared with the unreacted sample (Fig. 4). The mean hardness value of the unreacted sample was 241 MPa compared with ~60 MPa measured in the samples exposed to brine and de-ionized water. All hardness values from reacted samples were less than the minimum value from the unreacted sample. Hardness values of unreacted samples were consistent with values reported by others for cement paste (Igarashi *et al.*, 1996). Hardness

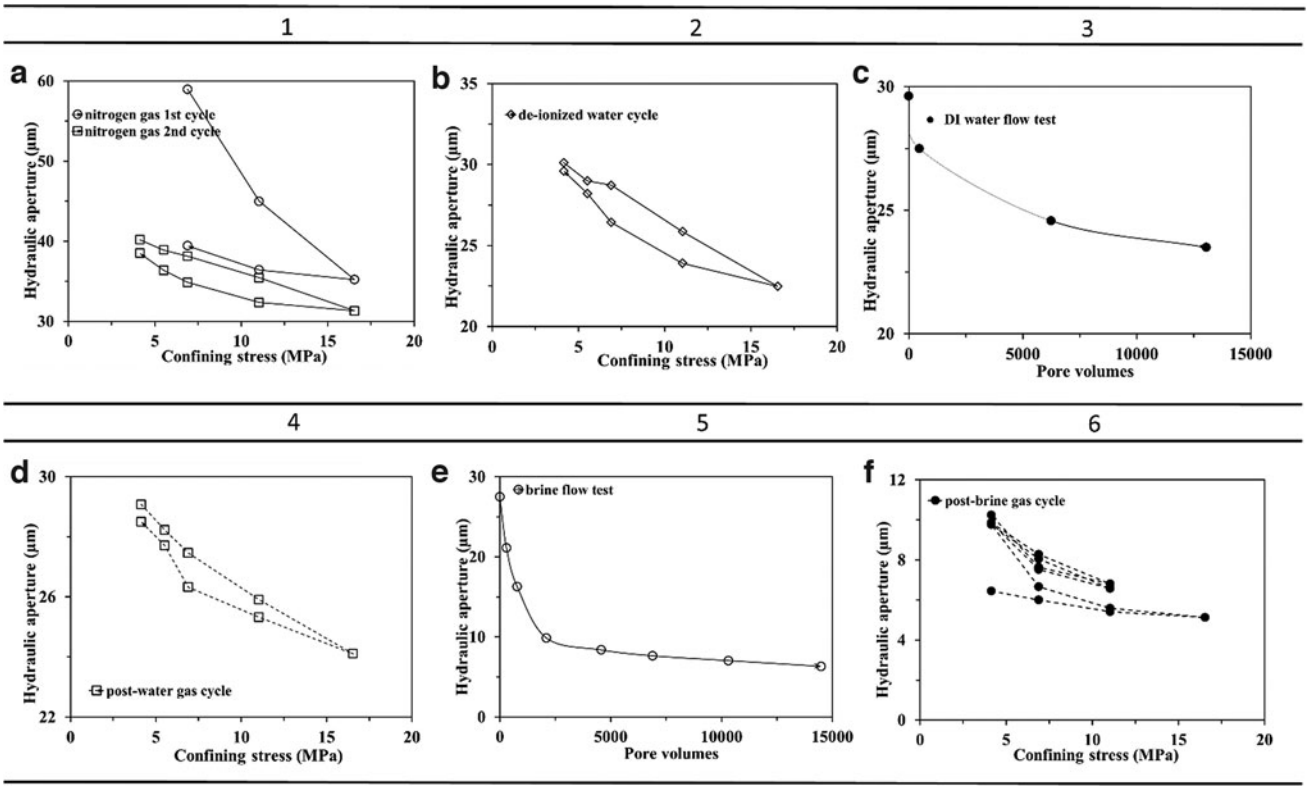

FIG. 3. Hydraulic apertures of cement fracture measured during flow tests under range of confining stresses and fluids. **(a)** Response to confining stress for first and second nitrogen gas cycle. **(b)** Response to confining stress between 4.1 and 16.5 MPa using de-ionized water. **(c)** Response to constant a flow of de-ionized water with at 11 MPa. **(d)** Response to confining stress between 4.1 and 16.5 MPa using nitrogen gas. **(e)** Response to a constant brine flow at 11 MPa, **(f)** Response to confining stress between 4.1 and 16.5 MPa using nitrogen gas. Note that different scales were used for better resolution of the data presented.

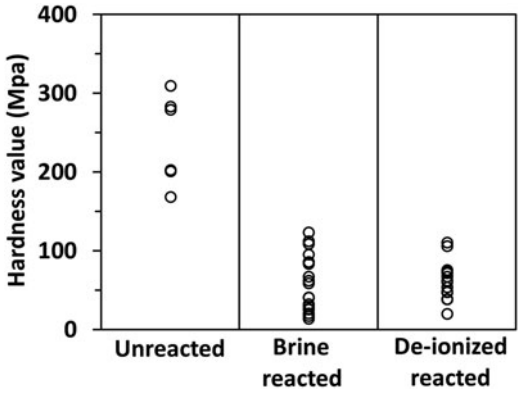

FIG. 4. Hardness values from fractured cement surfaces of unreacted (control) sample, brine-reacted (flow test) sample, and de-ionized water-reacted sample.

values have been linearly correlated to strength and inversely correlated to porosity (Beaudoin and Feldman, 1975), suggesting that the fracture surfaces that were exposed to brine and de-ionized water had a lower strength and greater porosity than the unreacted cement.

There was no discernable difference between the hardness values of samples reacted with de-ionized water and the flow test sample (reacted sequentially with nitrogen, de-ionized water, and brine). However, the differences in chemical composition indicated by our solid analyses data for experiments reacted with de-ionized water and brine suggest that dissolution and surface precipitation reaction mechanisms that decreased the hardness under these experimental conditions are different. The salts contained in the synthetic brine, particularly $NaHCO_3$, may have reacted with the wellbore surface. Bicarbonate is well known for solubilizing, complexing, and precipitating a wide range of metals and salts (Benjamin, 2014).

The solid phases identified by XRD analyses such as portlandite [$Ca(OH)_2$], haturite (Ca_3SiO_6), calcite [$CaCO_3$], monticellite [$CaMgSiO_4$], have different quantities in the unreacted cement, de-ionized reacted cement, and brine reacted cement (shown hereunder in the XRD analyses; Table 2). Lower hardness values and the corresponding decrease in strength and increase in porosity have been attributed to leaching of Ca from cement (Schwotzer *et al.*, 2010; Hou *et al.*, 2014). De-ionized water, on the contrary, is free of salts (undersaturated) and causes the dissolution of a readily releasable fraction of calcium in the wellbore cement into the liquid phase.

Flow of de-ionized water and brine through fractured cement caused a decrease in hardness and hydraulic aperture. To better understand the interaction between mechanical and chemical processes, further aqueous chemical analyses were performed on water samples collected from experiments reacting fractured cement with de-ionized water and brine.

Chemical Reactivity Experiments on Fractured Cement

Calcium release in liquid flow experiments

During the flow tests given in Fig. 3c and e, we measured the concentration of Ca in the effluent. Figure 5 shows the effluent Ca concentrations and flow tests as a function of pore volume with de-ionized water. The concentration of Ca stabilized at ~9,000 mg/L (224.55 mM) after the injection of 1,900 pore volumes (Fig. 5a), whereas it reached ~150 mg/L (3.74 mM) after ~500 pore volumes of de-ionized water passed through and decreased to ~75 mg/L (1.87 mM) (Fig. 5b). The hydraulic aperture decreased from 27.5 to 6.3 μm (4.3×) in the sample exposed to brine compared with 29.6–23.5 (1.26×) in the sample exposed to de-ionized water.

Chemical speciation calculations using MINEQL and FLOTRAN indicated that the experimental solution used in

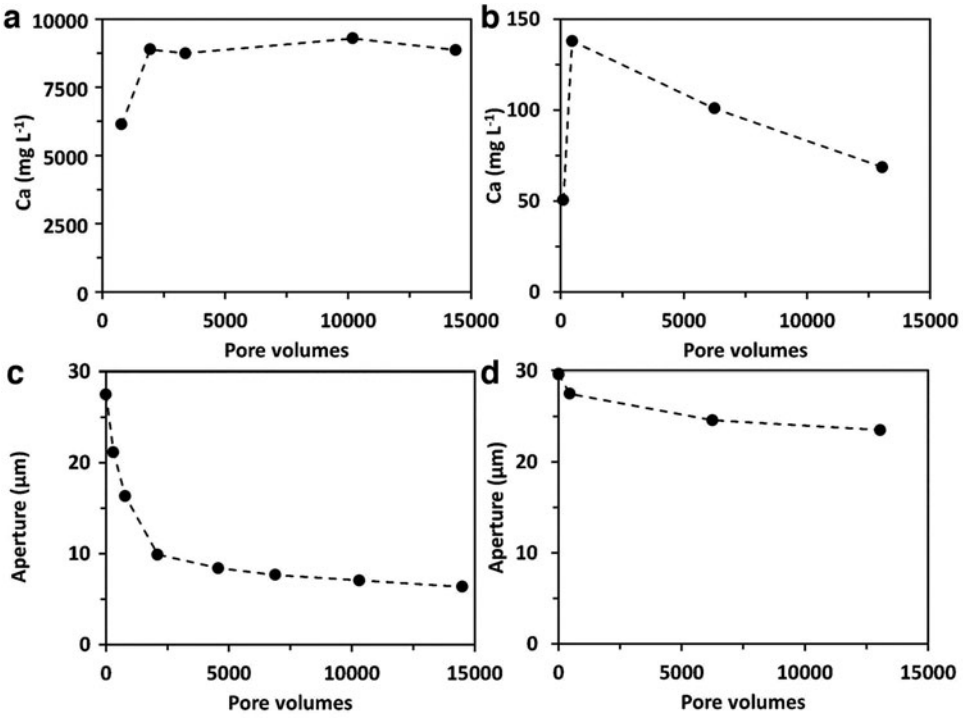

FIG. 5. Calcium (Ca) concentration of the effluent from the flow test after reaction of cement with brine **(a)** and de-ionized water **(b)**; and hydraulic aperture response to flow of brine **(c)** and de-ionized water **(d)** under sustained confining stress of 11 MPa.

this study is supersaturated with respect to $CaCO_3$ solids calcite and aragonite (Table 3). These simulations also indicated that the solution was undersaturated with respect to $Ca(OH)_2$ solids portlandite and lime. Note that the SIs obtained using parameters of the specific interaction model with MINEQL and Pitzer model with FLOTRAN were similar and consistent. Slight differences in equilibrium constants used in the calculations partially account for the differences in SIs.

Our results indicate that the supersaturation of $CaCO_{3(s)}$ in the brine caused closure of the fractures in the cement and the reduction in hydraulic aperture. The major source of Ca comes from the brine given that the soluble Ca concentration is ~9,000 mg/L (224.55 mM) during the flow test, compared with only ~150 mg/L (3.74 mM) of Ca released in the flow test when reacted with de-ionized water. The de-ionized water reaction (pH 5.66) with cement serves as a baseline of readily releasable Ca caused by portlandite dissolution. Such results suggest that supersaturated brines with respect to $CaCO_{3(s)}$ may decrease fluid leakage into the environment by sealing cement fractures.

In field conditions, actual brines are complex solutions, that is, contain high concentrations of total dissolved solids and are rich in salts and organic matter (Lauer *et al.*, 2016). Brines rich in salts and CO_2 could promote $CaCO_3$ precipitation replacing portlandite and reducing fluid leakage as the fracture aperture decreases. However, intense alterations of the wellbore surface may enable leakage of fluids into the environment and decrease sealing reactions (Garcia-Rios and Gouze, 2018). Additional solid analyses were conducted to characterize morphology, element composition, and mineralogy of unreacted and reacted solids from these experiments.

Characterization of Unreacted and Reacted Solids

SEM/EDX: Morphology and elemental content

Figure 6 shows the analyses of SEM images and EDX spectra (signal corresponding to the top 1 μm depth from the surface) for different regions in unreacted cement samples and in those reacted from the flow tests (reacted sequentially with nitrogen, de-ionized water, and brine) and the sample reacted only with de-ionized water. Differences in morphology and elemental composition were observed for the flow test sample compared with unreacted and reacted only with de-ionized water likely owing to chemical precipitation over the course of the experiments. Data from SEM and EDX analyses for unreacted cement samples indicate that Ca was predominant (Fig. 6a, b). Small crystals were observed in the SEM images for areas with hardness values >250 MPa in samples reacted with de-ionized water; Ca and Si were predominant elements as indicated in the EDX spectra (Fig. 6c, d).

In contrast, the morphology of areas with hardness values lower than 100 MPa resembles that of unreacted cement, but with layers of smaller sized crystals containing Ca and limited Si (Fig. 6e, f). Fractured cement from the flow test sample (reacted sequentially with nitrogen, de-ionized water, and brine) with hardness values >250 MPa showed precipitates with Ca as the predominant element and lower concentrations of Mg and Si (Fig. 6g, h). Fractured cement from the flow test sample with hardness values <100 MPa also showed Ca as the predominant element and lower concentrations of Mg, Al, Si, Fe, and Na (Fig. 6i, j). Additional XRD analyses were conducted to identify the bulk mineralogical composition of these solids.

X-ray diffraction: Mineralogical analyses

The XRD data for unreacted fractured cement and reacted with de-ionized water and brine are summarized in Table 2. The main minerals identified in the bulk of unreacted and reacted samples with de-ionized water and brine are portlandite [$Ca(OH)_2$], haturite (Ca_3SiO_6), calcite [$CaCO_3$], monticellite [$CaMgSiO_4$], $CaAl_4Si_2O_{11}$, periclase [MgO], and brownmillerite [Ca_2FeAlO_5]. A component for amorphous phases was also included in the quantitative analyses and detected in all samples.

Unreacted and reacted fractured cement samples with de-ionized water (pH 5.6) showed a similar mineralogy. However, certain differences were observed with a higher content of calcite in samples reacted with de-ionized water (14.3%) with hardness <100 MPa, compared with that observed in unreacted samples (10.9%) and in those reacted with de-ionized water with hardness >250 MPa (10.7%). In addition, a 4.6% weight portlandite was observed in samples reacted with de-ionized water at hardness <100 MPa compared with 9.7–10.4% weight portlandite in unreacted and reacted samples with de-ionized water at hardness >250 MPa. This slight decrease in portlandite content in the reacted sample at lower hardness is owing to mineral dissolution, which is related to the increase of Ca in solution (as high as 140 mg/L) (Fig. 5b).

The fractured cement sample from the flow test (reacted sequentially with nitrogen, de-ionized water, and brine) showed the most noticeable changes in mineralogical

Table 3. Solid Saturation Indices Obtained from Chemical Equilibrium Simulations Using MINEQL and FLOTRAN Based on the Brine Composition Used for This Study

Mineral	*Formula*[a]	K[b] *(MINEQL)*	K[b] *(FLOTRAN)*	*SIs (MINEQL)*	*SIs (FLOTRAN)*
Calcite	$CaCO_{3(s)}$	8.48	8.48	1.84	1.83
Aragonite	$CaCO_{3(s)}$	8.30	8.34	1.66	1.69
Portlandite	$Ca(OH)_{2(s)}$	−22.80	−22.55	−6.69	−7.14
Lime	$Ca(OH)_{2(s)}$	−32.69	−32.58	−16.58	−17.11

[a]Note that the information provided corresponds to the following reactions:
$Ca^{2+} + CO_3^{2-} = CaCO_{3(s)}$.
$Ca^{2+} - 2H^+ + 2H_2O = Ca(OH)_{2(s)}$.
[b]K is the chemical equilibrium constant used for the simulations with MINEQL and FLOTRAN.
SIs, saturation indices.

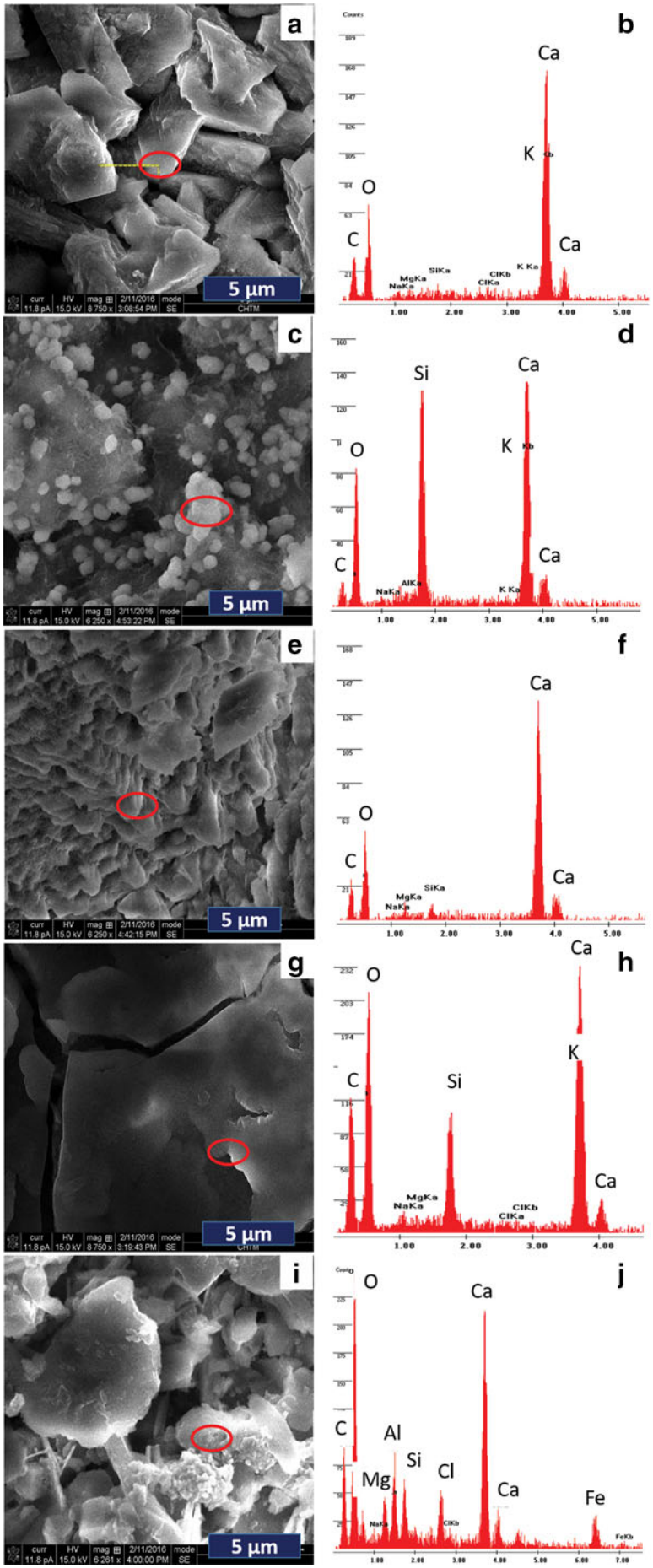

FIG. 6. SEM Image and EDX Spectra. **(a, b)** Unreacted fracture cement surface. **(c, d)** Fractured cement with hardness values >250 MPa reacted with de-ionized water. **(e, f)** Fractured cement with hardness values <100 MPa reacted with de-ionized water. **(g, h)** Fractured cement with hardness values >250 MPa from the flow test (reacted sequentially with nitrogen, de-ionized water and brine). **(i, j)** Fractured cement with hardness values <100 MPa from the flow test.

content. Fractured cement samples from the flow test contained from 2.2 to 2.5 times more calcite than unreacted samples and 1.71–2.6 times more calcite than samples reacted only with de-ionized water (Table 2). Higher contents of calcite detected by XRD and precipitates with high Ca signals observed in SEM/EDX suggests that chemical precipitation occurred in the surface of the fractured cement sample from the flow test. Calcite precipitation likely caused the fourfold decrease in hydraulic aperture in the fractured cement sample from the flow test.

The supersaturation of the brine solution with respect to $CaCO_{3(s)}$ and undersaturation with respect to portlandite appears to have led to the reduction of the hydraulic aperture and fracture permeability. The dissolution and precipitation of portlandite, swelling of calcium silica hydrate (C–S–H), hydration of nonreacted cement, and adsorption of water can decrease cement permeability (Loosveldt *et al.*, 2002; Yurtdas *et al.*, 2011b; Tao *et al.*, 2016). Walsh *et al.* (2014) determined that properties such as strength, hardness, and elastic moduli changed in agreement to alterations in cement composition. Dissolution and precipitation can clog pores and decrease porosity limiting the penetration of fluid through the pores (Brunet *et al.*, 2013; Iyer *et al.*, 2017; Nguyen *et al.*, 2020; Plattenberger *et al.*, 2020). Leaching of calcium from portlandite can increase porosity and hydraulic diffusivity (Marchand *et al.*, 2001; Phung *et al.*, 2016). Duguid and Scherer (2010) found that calcium-saturated brine did not degrade or decrease the mechanical properties of cement suggesting that water saturated with calcium prevents the dissolution of portlandite and decalcification of calcium silica hydrate (C–S–H). Precipitates that consist of amorphous solid phases not detectable by XRD may also be affecting the physical properties of the fractured cement surface. Future research is necessary to better understand the effect of precipitation and dissolution reactions on the physical properties of fractured cement.

Conclusions

Our findings indicate that hydraulic aperture decreased the most in fractured cement samples from the flow test (reacted sequentially with nitrogen, de-ionized water, and brine) because of the precipitation of $CaCO_3$ (e.g., calcite and aragonite) solids. An effluent concentration of $\sim$9,000 mg/L (224.55 mM) of Ca was measured during the flow test when reacted with brine, compared with only $\sim$150 mg/L (3.74 mM) of Ca released in the flow test when reacted with de-ionized water. This result indicates that the readily released Ca from the reaction of cement with de-ionized water is at least two orders of magnitude lower than the Ca concentration present in the supersaturated brine with respect to $CaCO_{3(s)}$ and that released from dissolution of portlandite, which is not possible to distinguish in this experiment.

Although brine and de-ionized water similarly affected the cement hardness (average values $\sim$60 MPa), spectroscopy (SEM/EDX) and XRD solid analyses confirmed the increase in calcite precipitation after reaction of cement with brine. Our data suggest that brine can promote $CaCO_{3(s)}$ precipitation that causes sealing in cement fractures. Sealing can potentially decrease leakages and the undesired impact of hydrocarbon contaminants on aquifers and atmosphere. Future research should investigate the effect of hardness on hydraulic aperture and chemical composition under conditions that are relevant for resource extraction applications such as hydraulic fracturing. This knowledge will help understand the effect of complex chemical reactions in waters with elevated ionic strength that could affect flow transport from fractured cement into the environment. This has relevant implications for oil and gas extraction.

Disclaimer

Any opinion, findings, and conclusions or recommendations expressed in this material are those of the authors(s) and do not necessarily reflect the views of the National Science Foundation.

Author Disclosure Statement

No competing financial interests exist.

Funding Information

This work was supported by the National Science Foundation through the University of New Mexico Center for Water and the Environment (CREST Grant Nos. 1345169 and 1914490).

References

Agostini, F., Lafhaj, Z., Skoczylas, F., and Loodsveldt, H. (2007). Experimental study of accelerated leaching on hollow cylinders of mortar. *Cement Concrete Res.* 37, 71.

American Society for testing and Materials (2014). *ASTM C305-14, Standard Practice for Mechanical Mixing of Hydraulic Cement Pastes and Mortars of Plastic Consistency.* West Conshohocken, PA, USA: ASTM International.

Bandis, S., Lumsden, A., and Barton, N. (1983). Fundamentals of rock joint deformation. *Int. J. Rock. Mech. Min.* 20, 249.

Baur, I., Keller, P., Mavrocordatos, D., Wehrli, B., and Johnson, C.A. (2004). Dissolution-precipitation behaviour of ettringite, monosulfate, and calcium silicate hydrate. *Cement Concrete Res.* 34, 341.

Beaudoin, J.J., and Feldman, R.F. (1975). A study of mechanical properties of autoclaved Calcium silicate systems. *Cement Concrete Res.* 5, 103.

Benjamin, M.M. (2014). *Water Chemistry*. Long Grove, IL, USA: Waveland Press, Inc.

Brunet, J.-P.L., Li, L., Karpyn, Z.T., Kutchko, B.G., Strazisar, B., and Bromhal, G. (2013). Dynamic evolution of cement composition and transport properties under conditions relevant to geological carbon sequestration. *Energy Fuels* 27, 4208.

Carde, C., and Francois, R. (1999). Modelling the loss of strength and porosity increase due to the leaching of cement pastes. *Cement Concrete Comp.* 21, 181.

Carey, J.W., and Lichtner, P.C. (2009). Computational studies of two-phase cement-co_2-brine interaction in Wellbore environments. In *International Conference on Carbon Dioxide Capture, Storage and Utility*. Society of Petroleum Engineers, San Diego, CA, USA, p. 12.

Carey, J.W., Svec, R., Grigg, R., Zhang, J., and Crow, W. (2010). Experimental investigation of wellbore integrity and CO_2–brine flow along the casing–cement microannulus. *Int. J. Greenh. Gas Con.* 4, 272.

Carroll, S., Carey, J.W., Dzombak, D., Huerta, N.J., Li, L., Richard, T., Um, W., Walsh, S.D.C., and Zhang, L. (2016).

Review: Role of chemistry, mechanics, and transport on well integrity in CO_2 storage environments. *Int. J. Greenh. Gas Con.* 49, 149.

Chen, Y.-F., Zhou, J.-Q., Hu, S.-H., Hu, R., and Zhou, C.-B. (2015). Evaluation of Forchheimer equation coefficients for non-Darcy flow in deformable rough-walled fractures. *J. Hydrol.* 529, 993.

De Andrade, J., Torsaeter, M., Todorovic, J., Opedal, N., Stroisz, A., and Vralstad, T. (2014). Influence of casing centralization on cement sheath integrity during thermal cycling. In *IADC/SPE Drilling Conference Exhibition.* Richardson, TX: Society of Petroleum Engineers.

Deng, H., and Peters, C.A. (2019). Reactive transport simulation of fracture channelization and transmissivity evolution. *Environ. Eng. Sci.* 36, 90.

Deng, H., Steefel, C., Molins, S., and DePaolo, D. (2018). Fracture evolution in multimineral systems: The role of mineral composition, flow rate, and fracture aperture heterogeneity. *ACS Earth Space Chem.* 2, 112.

Duguid, A., and Scherer, G.W. (2010). Degradation of oilwell cement due to exposure to carbonated brine. *Int. J. Greenh. Gas Con.* 4, 546.

Elkhoury, J.E., Ameli, P., and Detwiler, R.L. (2013). Dissolution and deformation in fractured carbonates caused by flow of CO_2-rich brine under reservoir conditions. *Int. J. Greenh. Gas Con.* 16, S203.

Garcia-Rios, M., and Gouze, P. (2018). Time-space characterization of Wellbore-cement alteration by CO_2-rich brine. *Geoscience* 8, 490.

Garcia-Rios, M., Luquot, L., Soler, J.M., and Cama, J. (2015). Influence of the flow rate on dissolution and precipitation features during percolation of CO2-rich sulfate solutions through fractured limestone samples. *Chem. Geol.* 414, 95.

Haluszczak, L.O., Rose, A.W., and Kump, L.R. (2013). Geochemical evaluation of flowback brine from Marcellus gas wells in Pennsylvania, USA. *Appl. Geochem.* 28, 55.

Hassanizadeh, S.M., and Gray, W.G. (1987). High velocity flow in porous media. *Transport Porous Med.* 2, 521.

Heathman, J., and East, Jr., L. (1992). Case histories regarding the application of microfine cements. In *SPE/IADC Drilling Conference*. Richardson, TX: Society of Petroleum Engineers.

Hou, P., Zhang, R., and Cheng, X. (2014). Case study of the gradient features of in situ concrete. *Case St. Constr. Mater.* 1, 154.

Huerta, N.J., Bryant, S.L., Strazisar, B.R., and Hesse, M. (2011). Dynamic alteration along a fractured cement/cement interface: Implications for long term leakage risk along a well with an annulus defect. *Energy Proc.* 4, 5398.

Huerta, N.J., Hesse, M.A., Bryant, S.L., Strazisar, B.R., and Lopano, C.L. (2012). Experimental evidence for self-limiting reactive flow through a fractured cement core: Implications for time-dependent wellbore leakage. *Environ. Sci. Technol.* 47, 269.

Huitt, J. (1956). Fluid flow in simulated fractures. *AIChE J.* 2, 259.

Igarashi, S., Bentur, A., and Mindess, S. (1996). Microhardness testing of cementitious materials. *Adv. Cem. Based Mater.* 4, 48.

Iyer, J., Walsh, S.D.C., Hao, Y., and Carroll, S.A. (2017). Incorporating reaction-rate dependence in reaction-front models of wellbore-cement/carbonated-brine systems. *Int. J. Greenh. Gas Con.* 59, 160.

Ju, Y., Wang, Y., Chen, J., Gao, F., and Wang, J. (2018). Adaptive finite element-discrete element method for numerical analysis of the multistage hydrofracturing of horizontal wells in tight reservoirs considering pre-existing fractures, hydromechanical coupling, and leak-off effects. *J Nat. Gas Sci. Eng.* 54, 266.

Kang, M., Kanno, C.M., Reid, M.C., Zhang, X., Mauzerall, D.L., Celia, M.A., Chen, Y.H., and Onstott, T.C. (2014). Direct measurements of methane emissions from abandoned oil and gas wells in Pennsylvania. *Proc. Natl. Acad. Sci. U.S.A.* 111, 18173.

Kutchko, B.G., Strazisar, B.R., Dzombak, D.A., Lowry, G.V., and Thaulow, N. (2007). Degradation of well cement by CO_2 under geologic sequestration conditions. *Environ. Sci. Technol.* 41, 4787.

Lauer, N.E., Harkness, J.S., and Vengosh, A. (2016). Brine spills associated with unconventional oil development in North Dakota. *Environ. Sci. Technol.* 50, 5389.

Lichtner, P.C., and Felmy, A.R. (2003). Estimation of Hanford SX tank waste compositions from historically derived inventories. *Comput. Geosci.* 29, 371.

Loosveldt, H., Lafhaj, Z., and Skoczylas, F. (2002). Experimental study of gas and liquid permeability of a mortar. *Cement Concrete Res.* 32, 1357.

Marchand, J., Bentz, D.P., Samson, E., and Maltais, Y. (2001). Influence of calcium hydroxide dissolution on the transport properties of hydrated cement systems. In J. Skalny, J. Gebauer, and I. Odler, (Eds)., *Reactions of Calcium Hydroxide in Concrete*. Westerville, OH, USA: American Ceramic Society, p. 113.

Marty, N.C., Tournassat, C., Burnol, A., Giffaut, E., and Gaucher, E.C. (2009). Influence of reaction kinetics and mesh refinement on the numerical modelling of concrete/clay interactions. *J. Hydrol.* 364, 58.

Mason, H.E., Du Frane, W.L., Walsh, S.D., Dai, Z., Charnvanichborikarn, S., and Carroll, S.A. (2013). Chemical and mechanical properties of wellbore cement altered by CO_2-rich brine using a multianalytical approach. *Environ. Sci. Technol.* 47, 1745.

Nguyen, P., Guthrie, G.D., and Carey, J.W. (2020). Experimental validation of self-sealing in wellbore cement fractures exposed to high-pressure, CO_2-saturated solutions. *Int. J. Greenh. Gas Con.* 100, 103112.

Phillips, A.J., Cunningham, A.B., Gerlach, R., Hiebert, R., Hwang, C., Lomans, B.P., Westrich, J., Mantilla, C., Kirksey, J., Esposito, R., and Spangler, L. (2016). Fracture sealing with microbially-induced calcium carbonate precipitation: A field study. *Environ. Sci. Technol.* 50, 4111.

Phung, Q.T., Maes, N., Jacques, D., De Schutter, G., and Ye, G. (2016). Investigation of the changes in microstructure and transport properties of leached cement pastes accounting for mix composition. *Cement Concrete Res.* 79, 217.

Plattenberger, D., Brown, T., Ling, F.T., Lyu, X., Fitts, J., Peters, C.A., and Clarens, A.F. (2020). Feasibility of using reactive silicate particles with temperature-responsive coatings to enhance the security of geologic carbon storage. *Int. J. Greenh. Gas Con.* 95, 102976.

Schecher, W.D., and McAvoy, D.C. (2007). *MINEQL+: A Chemical Equilibrium Modeling System; Version 4.6, 4.5 for Windows Workbook*. Hallowell, ME, USA: Environmental Research Software.

Schout, G., Griffioen, J., Hassanizadeh, S.M., de Lichtbuer, G.C., and Hartog, N. (2019). Occurrence and fate of methane leakage from cut and buried abandoned gas wells in the Netherlands. *Sci. Total Environ.* 659, 773.

Schwotzer, M., Scherer, T., and Gerdes, A. (2010). Protective or damage promoting effect of calcium carbonate layers on the

surface of cement based materials in aqueous environments. *Cement Concrete Res.* 40, 1410.

Sobolik, S.R., and Ehgartner, B.L. (2006). *Analysis of Salt and Analysis of Salt and Casing Fracture Mechanisms During Cavern Integrity Testing for SPR Salt Caverns.* S.N.L. SAND2007-1974. U.S. Department of Commerce. National Technical Information Service. Port Royal Rd Springfield, VA.

Spokas, K., Peters, C.A., and Pyrak-Nolte, L. (2018). Influence of rock mineralogy on reactive fracture evolution in carbonate-rich caprocks. *Environ. Sci. Technol.* 52, 10144.

Stormont, J.C., Fernandez, S.G., Taha, M.R., and Matteo, E.N. (2018). Gas flow through cement-casing microannuli under varying stress conditions. *Geomech. Energy Environ.* 13, 1.

Tao, Z., Fitts, J.P., and Clarens, A.F. (2016). Feasibility of carbonation reactions to control permeability in the deep subsurface. *Environ. Eng. Sci.* 33, 778.

Townsend-Small, A., Ferrara, T.W., Lyon, D.R., Fries, A.E., and Lamb, B.K. (2016). Emissions of coalbed and natural gas methane from abandoned oil and gas wells in the United States. *Geophys. Res. Lett.* 43, 2283.

VanBriesen, J.M., Small, M., Weber, C., and Wilson, J. (2010). Modelling chemical speciation: thermodynamics, kinetics and uncertainty. In: *Modelling of Pollutants in Complex Environmental Systems*, Vol. 2, ILM: St Albans, United Kingdom, p. 133.

Vengosh, A., Jackson, R.B., Warner, N., Darrah, T.H., and Kondash, A. (2014). A critical review of the risks to water resources from unconventional shale gas development and hydraulic fracturing in the United States. *Environ. Sci. Technol.* 48, 8334.

Walsh, S.D., Mason, H.E., Du Frane, W.L., and Carroll, S.A. (2014). Mechanical and hydraulic coupling in cement–caprock interfaces exposed to carbonated brine. *Int. J. Greenh. Gas Con.* 25, 109.

Wiprut, D., and Zoback, M. (2000). Constraining the stress tensor in the Visund field, Norwegian North Sea: Application to wellbore stability and sand production. *Int. J. Rock. Mech. Min.* 37, 317.

Witherspoon, P.A., Wang, J.S., Iwai, K., and Gale, J.E. (1980). Validity of cubic law for fluid flow in a deformable rock fracture. *Water Resour. Res.* 16, 1016.

Yurtdas, I., Xie, S., Burlion, N., Shao, J.-F., Saint-Marc, J., and Garnier, A. (2011a). Influence of chemical degradation on mechanical behavior of a petroleum cement paste. *Cement Concrete Res.* 41, 412.

Yurtdas, I., Xie, S.Y., Burlion, N., Shao, J.F., Saint-Marc, J., and Garnier, A. (2011b). Deformation and permeability evolution of petroleum cement paste subjected to chemical degradation under temperature. *Transport Porous Med.* 86, 719.

Zhang, M., and Bachu, S. (2011). Review of integrity of existing wells in relation to CO_2 geological storage: What do we know? *Int. J. Greenh. Gas Con.* 5, 826.

Zhang, Z., and Nemcik, J. (2013). Fluid flow regimes and nonlinear flow characteristics in deformable rock fractures. *J. Hydrol.* 477, 139.

Zhou, J.-Q., Hu, S.-H., Fang, S., Chen, Y.-F., and Zhou, C.-B. (2015). Nonlinear flow behavior at low Reynolds numbers through rough-walled fractures subjected to normal compressive loading. *Int. J. Rock. Mech. Min.* 80, 202.